Hydrol. Earth Syst. Sci. Discuss., 12, 7503–7540, 2015
www.hydrol-earth-syst-sci-discuss.net/12/7503/2015/
doi:10.5194/hessd-12-7503-2015

Hydrology and Earth System Sciences
Open Access
Discussions

Analysis of three-dimensional groundwater flow toward a radial collector well in a finite-extent unconfined aquifer

C.-S. Huang, J.-J. Chen, and H.-D. Yeh

Institute of Environmental Engineering, National Chiao Tung University, Hsinchu, Taiwan

Received: 14 June 2015 – Accepted: 26 July 2015 – Published: 6 August 2015

Correspondence to: H.-D. Yeh (hdyeh@mail.nctu.edu.tw)

Published by Copernicus Publications on behalf of the European Geosciences Union.

Abstract

This study develops a three-dimensional mathematical model for describing transient hydraulic head distributions due to pumping at a radial collector well (RCW) in a rectangular confined or unconfined aquifer bounded by two parallel streams and no-flow boundaries. The governing equation with a point-sink term is employed. A first-order free surface equation delineating the water table decline induced by the well is considered. The head solution for the point sink is derived by applying the methods of double-integral transform and Laplace transform. The head solution for a RCW is obtained by integrating the point-sink solution along the laterals of the RCW and then dividing the integration result by the sum of lateral lengths. On the basis of Darcy's law and head distributions along the streams, the solution for the stream depletion rate (SDR) can also be developed. With the aid of the head and SDR solutions, the sensitivity analysis can then be performed to explore the response of the hydraulic head to the change in a specific parameter such as the horizontal and vertical hydraulic conductivities, streambed permeability, specific storage, specific yield, lateral length and well depth. Spatial head distributions subject to the anisotropy of aquifer hydraulic conductivities are analyzed. A quantitative criterion is provided to identify whether groundwater flow at a specific region is 3-D or 2-D without the vertical component. In addition, another criterion is also given to allow the neglect of vertical flow effect on SDR. Conventional 2-D flow models can be used to provide accurate head and SDR predictions if satisfying these two criteria.

1 Introduction

The applications of a radial collector well (RCW) have received much attention in the aspects of water resource supply, groundwater remediation, and petroleum engineering since rapid advances in drilling technology. An average yield for the well approximates 27 000 m^3 day^{-1} (Todd and Mays, 2005). As compared to vertical wells, RCWs

HESSD
12, 7503–7540, 2015

require less operating cost, produce smaller drawdown, and have better efficiency of withdrawing water from thin aquifers. In addition, RCWs can extract water from an aquifer underlying obstacles such as buildings, but vertical wells cannot. Recently, Huang et al. (2012) reviewed semi-analytical and analytical solutions associated with RCWs. Since then, Yeh and Chang (2013) provided a valuable overview of articles associated with RCWs.

A variety of analytical models involving a horizontal well, a specific case of a RCW with a single lateral, in aquifers were developed (e.g., Park and Zhan, 2003; Hunt, 2005; Anderson, 2013). The flux along the well screen is commonly assumed to be uniform. The equation describing three-dimensional (3-D) flow is used. Kawecki (2000) developed analytical solutions of the hydraulic heads for the early linear flow perpendicular to a horizontal well and late pseudo-radial flow toward the middle of the well in confined aquifers. They also developed an approximate solution for unconfined aquifers on the basis of the head solution and an unconfined flow modification. The applicability of the approximate solution was later evaluated in comparison with a finite difference solution developed by Kawecki and Al-Subaikhy (2005). Zhan et al. (2001) presented an analytical solution for drawdown induced by a horizontal well in confined aquifers and compared the difference in the type curves produced by the well and by a vertical well. Zhan and Zlotnik (2002) developed a semi-analytical solution of drawdown due to pumping from a nonvertical well in an unconfined aquifer accounting for the effect of instantaneous drainage or delayed yield when the free surface declines. They discussed the influences of the length, depth, and inclination of the well on temporal drawdown distributions. Park and Zhan (2002) developed a semi-analytical drawdown solution considering the effects of a finite diameter, the wellbore storage, and a skin zone around a horizontal well in anisotropic leaky aquifers. They found that those effects cause significant change in drawdown at an early pumping period. Zhan and Park (2003) provided a general semi-analytical solution for pumping-induced drawdown in a confined aquifer, an unconfined aquifer on a leaky bottom, or a leaky aquifer below a water reservoir. Temporal drawdown distributions subject to the aquitard stor-

HESSD
12, 7503–7540, 2015

age effect were compared with those without that effect. Sun and Zhan (2006) derived a semi-analytical solution of drawdown due to pumping at a horizontal well in a leaky aquifer. A transient one-dimensional flow equation describing the vertical flow across the aquitard was considered. The derived solution was used to evaluate the Zhan and Park (2003) solution which assumed steady-state vertical flow in the aquitard.

Sophisticated numerical models involved in RCWs or horizontal wells were also reported. Steward (1999) applied the analytic element method to approximate 3-D steady-state flow induced by horizontal wells in contaminated aquifers. They discussed the relation between a pumping rate and the size of a polluted area. Chen et al. (2003) utilized the polygon finite difference method to deal with three kinds of seepage-pipe flows including laminar, turbulent, and transitional flows within a finite-diameter horizontal well. A sandbox experiment was also carried out to verify the prediction made by the method. Mohamad and Rushton (2006) used MODFLOW to predict flows inside an aquifer, from the aquifer to a horizontal well, and within the well. The predicted head distributions were compared with field data measured in Sarawak, Malaysia. Su et al. (2007) used the software TOUGH2 based on the integrated finite difference method to handle irregular configurations of several laterals of two RCWs installed beside the Russian River, Forestville, California and analyzed pumping-induced unsaturated regions beneath the river. Lee et al. (2012) developed a finite element solution with triangle elements to assess whether the operation of a RCW near Nakdong River in South Korea can induce riverbank filtration. They concluded that the well can be used for sustainable water supply at the study site. In addition, Rushton and Brassington (2013a) extended Mohamad and Rushton (2006) study by enhancing the Darcy-Weisbach formula to describe frictional head lose inside a horizontal well. The spatial distributions of predicted flux along the well revealed that the flux at the pumping end is four times of the magnitude of that at the far end. Later, Rushton and Brassington (2013b) applied the same model to a field experiment at the Seton Coast, northwest England.

Well pumping in aquifers near streams may cause groundwater-surface water interactions (e.g., Rodriguez et al., 2013; Chen et al., 2013; Zhou et al., 2013; Exner-

HESSD
12, 7503–7540, 2015

Kittridge et al., 2014; Flipo et al., 2014; Unland et al., 2014). The stream depletion rate (SDR), commonly used to quantify stream water filtration into the adjacent aquifer, is defined as the ratio of a filtration rate to a pumping rate. The SDR ranges from zero to a certain value which could be equal to or less than unity depending on situations (Zlotnik, 2004). Tsou et al. (2010) developed an analytical solution of SDR for a slanted well in confined aquifers adjacent to a stream treated as a constant-head boundary. They indicated that a horizontal well parallel to the stream induces the steady-state SDR of unity more quickly than a slanted well. Huang et al. (2011) developed an analytical SDR solution for a horizontal well in unconfined aquifers near a stream regarded as a constant-head boundary. Huang et al. (2012) provided an analytical solution for SDR induced by a RCW in unconfined aquifers adjacent to a stream with a low-permeability streambed treated as the Robin condition. The influence of the configuration of laterals on temporal SDR and spatial drawdown distributions was analyzed. Recently, Huang et al. (2014) gave an exhaustive review on analytical and semi-analytical SDR solutions and classified these solutions into two categories. One grouped the solutions involving two-dimensional (2-D) flow toward a fully-penetrating vertical well according to aquifer types and stream treatments. The other organized the solutions involving 3-D and quasi 3-D flows in the lights of aquifer types, well types, and stream treatments.

At present, existing analytical solutions associated with flow toward a RCW in unconfined aquifers have involved laborious calculation (Huang et al., 2012) and predicted approximate results (Hantush and Papadopoulos, 1962). The Huang et al. (2012) solution involves numerical integration of a triple integral in predicting the hydraulic head and a quintuple integral in predicting SDR. The integrand is expressed in terms of an infinite series expanded by roots of nonlinear equations. The integration variables are related to those roots. The application of their solution is therefore limited to those who are familiar with numerical methods. In addition, the accuracy of the Hantush and Papadopoulos (1962) solution is limited to some parts of a pumping period; that is, it gives accurate drawdown predictions at early and late times but divergent ones at middle time.

HESSD
12, 7503–7540, 2015

The objective of this study is to present new analytical solutions of the head and SDR, which overcome the above-mentioned limitations, for 3-D flow toward a RCW. A mathematical model is built to describe 3-D spatiotemporal hydraulic head distributions in a rectangular unconfined aquifer bounded by two parallel streams and by the no-flow stratums in the other two sides. The transient 3-D groundwater flow equation with a point-sink term is considered. The first-order free surface equation is used to describe water table decline due to pumping. The Robin boundary conditions are adopted to describe fluxes across the low-permeability streambeds connecting the aquifer and streams. The head solution for a point sink is derived by the methods of Laplace transform and double-integral transform. The analytical head solution for a RCW is then obtained by integrating the point-sink solution along the well and dividing the integration result by the total lateral length. The RCW head solution is expressed in terms of a triple series expanded by eigenvalues which can be obtained by a numerical algorithm such as Newton's method. On the basis of Darcy's law and the RCW head solution, the SDR solution can then be obtained in terms of a double series with fast convergence. With the aid of both solutions, the sensitivity analysis is performed to investigate the response of the hydraulic head to the change in each of aquifer parameters. The spatial distributions of the head and streamline are discussed. Spatial head distributions subject to the anisotropy of aquifer hydraulic conductivities are analyzed. The influences of the vertical flow and well depth on temporal SDR distributions are investigated. Moreover, temporal SDR distributions induced by a RCW and a fully penetrating vertical well in confined aquifers are also compared. A quantitative criterion is provided to identify whether groundwater flow at a specific region is 3-D or 2-D without the vertical component. In addition, another criterion is also given to judge the suitability of neglecting the vertical flow effect on SDR.

HESSD
12, 7503–7540, 2015

2 Methodology

2.1 Mathematical model

Consider a RCW in a rectangular unconfined aquifer bounded by two parallel streams and no-flow stratums as illustrated in Fig. 1. The symbols for variables and parameters are defined in Table 1. The origin of the Cartesian coordinate is located at the lower left corner. The aquifer domain falls in the range of $0 \le \times \le w_x$, $0 \le y \le w_y$, and $-H \le z \le 0$. The RCW consists of a caisson and several laterals, each of which extends finitely with length L_k and counterclockwise with angle θ_k where $k \in 1, 2, \ldots$ or N. The caisson is located at (x_0, y_0), and the surrounding laterals are at depth z_0 measured from water table.

First of all, a mathematical model describing 3-D flow toward a point sink in the aquifer is proposed. The equation describing 3-D hydraulic head distribution $h(x, y, z, t)$ subject to a point sink is expressed as

$$K_x \frac{\partial^2 h}{\partial x^2} + K_y \frac{\partial^2 h}{\partial y^2} + K_z \frac{\partial^2 h}{\partial z^2} = S_s \frac{\partial h}{\partial t} + Q\,\delta(x - x'_0)\delta(y - y'_0)\delta(z + z'_0) \quad (1)$$

where δ is the Dirac delta function, the second term on the right-hand side (RHS) indicates the point sink, and Q is positive for pumping and negative for injection. By choosing water table as a reference datum where the elevation head is set to zero, the initial condition can therefore be denoted as

$$h = 0 \text{ at } t = 0 \quad (2)$$

Note that Eq. (2) introduces negative hydraulic head for pumping, and the absolute value of the head equals drawdown.

The aquifer boundaries at $x = 0$ and $x = w_x$ are considered to be impermeable and thus expressed as

$$\partial h/\partial x = 0 \text{ at } x = 0 \quad (3)$$

HESSD
12, 7503–7540, 2015

and

$$\partial h/\partial x = 0 \text{ at } x = w_x \tag{4}$$

The use of Eqs. (3) and (4) have two advantages as mentioned in Huang et al. (2014). One is that the integrations in Eqs. (43), (50) and (51) can be done analytically. The other is that the series term of $2\sum_{m=1}^{\infty}\phi_{m,n}X_{m,n}\cos(\alpha_m\bar{x})$ in Eq. (31) of the head solution disappears when estimating the SDR from two parallel streams (i.e., Eqs. 50 and 51).

Streambed permeability is usually less permeable than the adjacent aquifer formation. The streams with low-conductivity streambeds are therefore treated as the Robin boundary conditions for describing the fluxes across the streambeds as

$$K_y\frac{\partial h}{\partial y} - \frac{K_1}{b_1}h = 0 \text{ at } y = 0 \tag{5}$$

and

$$K_y\frac{\partial h}{\partial y} + \frac{K_2}{b_2}h = 0 \text{ at } y = w_y \tag{6}$$

The free surface equation describing the water table decline is written as

$$K_x\left(\frac{\partial h}{\partial x}\right)^2 + K_y\left(\frac{\partial h}{\partial y}\right)^2 + K_z\left(\frac{\partial h}{\partial z}\right)^2 - K_z\frac{\partial h}{\partial z} = S_y\frac{\partial h}{\partial t} \text{ at } z = h \tag{7}$$

Yeh et al. (2010) indicated that the effect of the second-order terms on the change in water table is generally ignorable. Nyholm et al. (2002) stated that saturated aquifer thickness can be assumed constant when water table decline is smaller than 10 % of the initial aquifer thickness (i.e., $|h| < 0.1H$). Equation (7) is thus linearized by neglecting the second-order terms and replacing $z = h$ with $z = 0$ as

$$K_z\frac{\partial h}{\partial z} = -S_y\frac{\partial h}{\partial t} \text{ at } z = 0 \tag{8}$$

HESSD
12, 7503–7540, 2015

The bottom of the aquifer is considered as the no-flow boundary condition denoted as

$$\partial h/\partial z = 0 \text{ at } z = -H \tag{9}$$

Dimensionless variables and parameters are listed in Table 1 in which the superscript bar denotes a dimensionless symbol. Equation (1) can be written as

$$\kappa_x \frac{\partial^2 \bar{h}}{\partial \bar{x}^2} + \frac{\partial^2 \bar{h}}{\partial \bar{y}^2} + \kappa_z \frac{\partial^2 \bar{h}}{\partial \bar{z}^2} = \frac{\partial \bar{h}}{\partial \bar{t}} + \delta(\bar{x} - \bar{x}'_0)\delta(\bar{y}' - \bar{y}'_0)\delta(\bar{z} + \bar{z}'_0) \tag{10}$$

Similarly, the initial and boundary conditions are expressed as

$$\bar{h} = 0 \text{ at } \bar{t} = 0 \tag{11}$$

$$\partial \bar{h}/\partial \bar{x} = 0 \text{ at } \bar{x} = 0 \tag{12}$$

$$\partial \bar{h}/\partial \bar{x} = 0 \text{ at } \bar{x} = \bar{w}_x \tag{13}$$

$$\partial \bar{h}/\partial \bar{y} - \kappa_1 \bar{h} = 0 \text{ at } \bar{y} = 0 \tag{14}$$

$$\partial \bar{h}/\partial \bar{y} + \kappa_2 \bar{h} = 0 \text{ at } \bar{y} = \bar{w}_y \tag{15}$$

$$\frac{\partial \bar{h}}{\partial \bar{z}} = -\frac{\gamma}{\kappa_z} \frac{\partial \bar{h}}{\partial \bar{t}} \text{ at } \bar{z} = 0 \tag{16}$$

and

$$\partial \bar{h}/\partial \bar{z} = 0 \text{ at } \bar{z} = -1 \tag{17}$$

2.2 Head solution for point sink

The model, Eqs. (10)–(17), reduces to an ordinary differential equation (ODE) with two boundary conditions in terms of $\bar{z}$ after taking Laplace transform and double-integral transform. One can refer to Appendix A for the definition of the latter transform. The first-order differential operator $\partial/\bar{t}$ in Eqs. (10) and (16) can be converted

HESSD
12, 7503–7540, 2015

to the Laplace parameter p after taking Laplace transform. Likewise, the second-order differential operators $\partial^2/\bar{x}^2$ and $\partial^2/\bar{y}^2$ in Eq. (10) can be converted to parameters after taking double-integral transform. In turn, Eq. (10) becomes a second-order ODE defined by

$$\kappa_z \frac{\partial^2 \widetilde{h}}{\partial \bar{z}^2} - (\kappa_x \alpha_m^2 + \beta_n^2 + p)\widetilde{h} = \cos(\alpha_m \bar{x}_0')\, K(\bar{y}_0')\, \delta(\bar{z} + \bar{z}_0')/p \tag{18}$$

where $\widetilde{h}$ is the transformed hydraulic head, $(m, n) \in 1, 2, 3, \ldots \infty$, $\alpha_m = m\pi/\bar{w}_x$, $K(\bar{y}_0')$ is defined by Eq. (A2) with $\bar{y} = \bar{y}_0'$, and β_n are eigenvalues equaling the roots of the following equation as (Latinopoulos, 1985)

$$\tan\left(\beta_n \bar{w}_y\right) = \frac{\beta_n(\kappa_1 + \kappa_2)}{\beta_n^2 - \kappa_1\, \kappa_2} \tag{19}$$

The method to determine the roots is discussed in Sect. 2.3.

On the basis of those two transforms, Eqs. (16) and (17), respectively, yield

$$\frac{\partial \widetilde{h}}{\partial \bar{z}} = -\frac{p\,\gamma}{\kappa_z}\widetilde{h} \text{ at } \bar{z} = 0 \tag{20}$$

and

$$\partial \widetilde{h}/\partial \bar{z} = 0 \text{ at } \bar{z} = -1 \tag{21}$$

Equation (18) can be separated into two homogeneous ODEs as

$$\kappa_z \frac{\partial^2 \widetilde{h}_a}{\partial \bar{z}^2} - (\kappa_x \alpha_m^2 + \beta_n^2 + p)\widetilde{h}_a = 0 \text{ for } -\bar{z}_0' \le \bar{z} \le 0 \tag{22}$$

and

$$\kappa_z \frac{\partial^2 \widetilde{h}_b}{\partial \bar{z}^2} - (\kappa_x \alpha_m^2 + \beta_n^2 + p)\widetilde{h}_b = 0 \text{ for } -1 \le \bar{z} \le -\bar{z}_0' \tag{23}$$

HESSD
12, 7503–7540, 2015

where h_a and h_b, respectively, represent the heads above and below $\bar{z} = -\bar{z}'_0$ where the point sink is located. Two continuity requirements should be imposed at $\bar{z} = -\bar{z}'_0$. The first is the continuity of the hydraulic head denoted as

$$\widetilde{h}_a = \widetilde{h}_b \text{ at } \bar{z} = -\bar{z}'_0 \tag{24}$$

The second describes the discontinuity of the flux due to point pumping represented by the Dirac delta function in Eq. (18). It can be derived by integrating Eq. (18) from $\bar{z} = -\bar{z}'_0-$ to $\bar{z} = -\bar{z}'_0+$ as

$$\frac{\partial \widetilde{h}_a}{\partial \bar{z}} - \frac{\partial \widetilde{h}_b}{\partial \bar{z}} = \frac{\cos(\alpha_m \bar{x}'_0) K(\bar{y}'_0)}{p \kappa_z} \text{ at } \bar{z} = -\bar{z}'_0 \tag{25}$$

Solving Eqs. (22) and (23) simultaneously with Eqs. (20), (21), (24), and (25) yields the Laplace-domain head solution as

$$\widetilde{h}_a(\alpha_m, \beta_n, \bar{z}, p) = \Omega\left(-\bar{z}'_0, \bar{z}, 1\right) \text{ for } -\bar{z}'_0 \le \bar{z} \le 0 \tag{26}$$

and

$$\widetilde{h}_b(\alpha_m, \beta_n, \bar{z}, p) = \Omega\left(\bar{z}, \bar{z}'_0, -1\right) \text{ for } -1 \le \bar{z} \le -\bar{z}'_0 \tag{27}$$

with

$$\Omega(a, b, c) = \frac{\cosh[(1+a)\lambda][-\kappa_z \lambda \cosh(b\lambda) + c\, p\gamma \sinh(b\lambda)] \cos(\alpha_m \bar{x}_0) K(\bar{y}_0)}{p \kappa_z \lambda (p\gamma \cosh\lambda + \kappa_z \lambda \sinh\lambda)} \tag{28}$$

$$\lambda = \sqrt{(\kappa_x \alpha_m^2 + \beta_n^2 + p)/\kappa_z} \tag{29}$$

where a, b, and c are arguments. Taking the inverse Laplace transform and double-integral transform to Eq. (28) results in Eq. (31). One is referred to Appendix B for the detailed derivation. A time-domain head solution for a point sink is therefore written as

$$\bar{h}(\bar{x}, \bar{y}, \bar{z}, \bar{t}) = \begin{cases} \Phi(-\bar{z}'_0,\ \bar{z},\ 1) for -\bar{z}'_0 \le \bar{z} \le 0 \\ \Phi(\bar{z},\ \bar{z}'_0,\ -1) for -1 \le \bar{z} \le -\bar{z}'_0 \end{cases} \tag{30}$$

HESSD
12, 7503–7540, 2015

with

$$\Phi(a,b,c) = \frac{2}{\bar{w}_x}\left\{\sum_{n=1}^{\infty}\left[\phi_n X_n + 2\sum_{m=1}^{\infty}\phi_{m,n}X_{m,n}\cos(\alpha_m \bar{x})\right]Y_n\right\} \tag{31}$$

$$\phi_{m,n} = \psi_{m,n} + \psi_{m,n,0} + \sum_{i=1}^{\infty}\psi_{m,n,i} \tag{32}$$

$$\psi_{m,n} = -\cosh[(1+a)\lambda_s]\cosh(b\lambda_s)\,/\,(\kappa_z\lambda_s\sinh\lambda_s) \tag{33}$$

$$\psi_{m,n,0} = \mu_{m,n,0}\cosh\left[(1+a)\lambda_0\right]\left[-\kappa_z\lambda_0\cosh(b\lambda_0) + c\,p_0\gamma\sinh(b\lambda_0)\right] \tag{34}$$

$$\psi_{m,n,i} = \nu_{m,n,i}\cos[(1+a)\lambda_i]\left[-\kappa_z\lambda_i\cos(b\lambda_i) + c\,p_i\gamma\sin(b\lambda_i)\right] \tag{35}$$

$$\mu_{m,n,0} = 2\exp\left(p_0\bar{t}\right)\,/\,\left\{p_0\left[(1+2\gamma)\kappa_z\lambda_0\cosh\lambda_0 + (p_0\gamma+\kappa_z)\sinh\lambda_0\right]\right\} \tag{36}$$

$$\nu_{m,n,i} = 2\exp\left(p_i\bar{t}\right)\,/\,\left\{p_i\left[(1+2\gamma)\kappa_z\lambda_i\cos\lambda_i + (p_i\gamma+\kappa_z)\sin\lambda_i\right]\right\} \tag{37}$$

$$Y_n = \frac{\beta_n\cos(\beta_n\bar{y}) + \kappa_1\sin(\beta_n\bar{y})}{(\beta_n^2+\kappa_1^2)[\bar{w}_y + \kappa_2/(\beta_n^2+\kappa_2^2)] + \kappa_1} \tag{38}$$

and

$$X_{m,n} = \cos(\alpha_m\bar{x}_0)\left[\beta_n\cos(\beta_n\bar{y}_0) + \kappa_1\sin(\beta_n\bar{y}_0)\right] \tag{39}$$

where $\lambda_s = \sqrt{\left(\kappa_x\alpha_m^2+\beta_n^2\right)/\kappa_z}$, $p_0 = \kappa_z\lambda_0^2 - \kappa_x\alpha_m^2 - \beta_n^2$, $p_i = -\kappa_z\lambda_i^2 - \kappa_x\alpha_m^2 - \beta_n^2$, ϕ_n and X_n equal $\phi_{m,\,n}$ and $X_{m,n}$ with $\alpha_m = 0$, respectively, and the eigenvalues λ_0 and λ_i are, respectively, the roots of the following equations:

$$e^{2\lambda_0} = \frac{-\gamma\kappa_z\lambda_0^2 + \kappa_z\lambda_0 + \gamma(\kappa_x\alpha_m^2+\beta_n^2)}{\gamma\kappa_z\lambda_0^2 + \kappa_z\lambda_0 - \gamma(\kappa_x\alpha_m^2+\beta_n^2)} \tag{40}$$

$$\tan\lambda_i = \frac{-\gamma(\kappa_z\lambda_i^2 + \kappa_x\alpha_m^2 + \beta_n^2)}{\kappa_z\lambda_i} \tag{41}$$

HESSD
12, 7503–7540, 2015

The determination for those eigenvalues is introduced in the next section. Notice that the solution consists of simple series expended by β_n, double series expended by β_n and λ_i (or α_m and β_n), and triple series expended by α_m, β_n and λ_i.

2.3 Evaluations for β_n, λ_0 and λ_i

Application of Newton's method with proper initial guesses to determine the eigenvalues β_n, λ_0 and λ_i has been proposed by Huang et al. (2014) and is briefly introduced herein. The eigenvalues are situated at the intersection points of the left-hand side (LHS) and RHS functions of Eq. (19) for β_n, Eq. (40) for λ_0, and Eq. (41) for λ_i. Hence, the initial guesses for β_n are considered as $\beta_n - \delta$ if $\beta_n > (\kappa_1 \kappa_2)^{0.5}$ and as $\beta_n + \delta$ if $\beta_n < (\kappa_1 \kappa_2)^{0.5}$ where $\beta_n = (2n-1)\pi/(2\bar{w}_y)$ and δ is a chosen small value such as 10^{-8} for avoiding being right at the vertical asymptote. In addition, the guess for λ_0 can be formulated as

$$\lambda_{0\,\text{initial}} = \delta + \left(-\kappa_z - \sqrt{\kappa_z[\kappa_z + 4\gamma^2(\kappa_x\alpha_m^2 + \beta_n^2)]}\right) \Big/ (2\gamma\kappa_z) \tag{42}$$

where the RHS second term represents the location of the vertical asymptote derived by letting the denominator of the RHS function in Eq. (40) to be zero. Moreover, the guessed value for λ_i is $(2i-1)\pi/2 + \delta$.

2.4 Head solution for radial collector well

The solution of head $\bar{h}_w(\bar{x}\bar{y}\bar{z}\bar{t})$ for a RCW can be derived by substituting $\bar{x}'_0 = \bar{x}_0 + \bar{l}\cos\theta$, $\bar{y}'_0 = 1 + \bar{l}\sin\theta$ and $\bar{z}'_0 = \bar{z}_0$ into the point-sink solution, Eq. (30), then by integrating the resultant solution along each lateral, and finally by dividing the integration result into the sum of lateral lengths. The derivation can be denoted as

$$\bar{h}_w\left(\bar{x},\bar{y},\bar{z},\bar{t}\right) = \left(\sum_{k=1}^{N}\bar{L}_k\right)^{-1}\int_0^{\bar{L}_k}\bar{h}\left(\bar{x},\bar{y},\bar{z},\bar{t}\right)d\bar{l} \tag{43}$$

HESSD
12, 7503–7540, 2015

Note that the integral in Eq. (43) can be done analytically because the aquifer is of finite extent with boundary conditions, Eqs. (12)–(15). After the integration, Eq. (43) can be expressed as

$$\bar{h}_w\left(\bar{x},\bar{y},\bar{z},\bar{t}\right) = \frac{1}{\sum_{k=1}^{N}\bar{L}_k}\sum_{k=1}^{N}\begin{cases}\Phi\left(-\bar{z}_0,\bar{z},1\right) \text{ for } -\bar{z}_0 \le \bar{z} \le 0\\ \Phi\left(\bar{z},\bar{z}_0,-1\right) \text{ for } -1 \le \bar{z} \le -\bar{z}_0\end{cases} \tag{44}$$

where Φ is defined by Eqs. (31)–(38), and X_n and $X_{m,n}$ in Eq. (31) are replaced, respectively, by

$$\hat{X}_{n,\,k} = -G_k/(\beta_n \sin\theta_k) \tag{45}$$

and

$$\hat{X}_{m,n,\,k} = \frac{\alpha_m F_k \cos\theta_k + \beta_n G_k \sin\theta_k}{\alpha_m^2\cos^2\theta_k - \beta_n^2\sin^2\theta_k} \tag{46}$$

with

$$F_k = \sin\left(X\alpha_m\right)\left[\beta_n\cos\left(Y\beta_n\right) + \kappa_1\sin\left(Y\beta_n\right)\right] - \sin\left(\bar{x}_0\alpha_m\right)\left(\beta_n\cos\beta_n + \kappa_1\sin\beta_n\right) \tag{47}$$

$$G_k = \cos\left(X\alpha_m\right)\left[\kappa_1\cos\left(Y\beta_n\right) - \beta_n\sin\left(Y\beta_n\right)\right] - \cos\left(\bar{x}_0\alpha_m\right)\left(\kappa_1\cos\beta_n - \beta_n\sin\beta_n\right) \tag{48}$$

where $X = \bar{x}_0 + \bar{L}_k\cos\theta_k$ and $Y = 1 + \bar{L}_k\sin\theta_k$. Notice that Eq. (45) is obtained by substituting $\alpha_m = 0$ into Eq. (46). When $\theta_k = 0$ or π, Eq. (45) reduces to Eq. (49) by applying L'Hospital's rule.

$$\hat{X}_{n,k} = \bar{L}_k\left(\beta_n\cos\beta_n + \kappa_1\sin\beta_n\right) \tag{49}$$

HESSD
12, 7503–7540, 2015

2.5 SDR solution for radial collector well

On the basis of Darcy's law and the head solution for a RCW, the SDR from streams 1 and 2 can be defined, respectively, as

$$SDR_1(\bar{t}) = -\int_{\bar{x}=0}^{\bar{x}=\bar{w}_x}\left(\int_{\bar{z}=-\bar{z}_0}^{\bar{z}=0}\frac{\partial \bar{h}_w}{\partial \bar{y}}d\bar{z} + \int_{\bar{z}=-1}^{\bar{z}=-\bar{z}_0}\frac{\partial \bar{h}_w}{\partial \bar{y}}d\bar{z}\right)d\bar{x} \text{ at } \bar{y}=0 \tag{50}$$

and

$$SDR_2(\bar{t}) = \int_{\bar{x}=0}^{\bar{x}=\bar{w}_x}\left(\int_{\bar{z}=-\bar{z}_0}^{\bar{z}=0}\frac{\partial \bar{h}_w}{\partial \bar{y}}d\bar{z} + \int_{\bar{z}=-1}^{\bar{z}=-\bar{z}_0}\frac{\partial \bar{h}_w}{\partial \bar{y}}d\bar{z}\right)d\bar{x} \text{ at } \bar{y}=\bar{w}_y \tag{51}$$

Again, the double integrals in both equations can be done analytically. Notice that the series expanded by m in Eq. (31) disappears due to the integration with respect to $\bar{x}$. The SDR_1 and SDR_2 are therefore expressed in terms of double series and given below:

$$SDR_1(\bar{t}) = -\frac{2}{\sum_{k=1}^{N}\bar{L}_k}\sum_{k=1}^{N}\sum_{n=1}^{\infty}\left(\hat{\psi}_n + \hat{\psi}_{n,0} + \sum_{i=1}^{\infty}\hat{\psi}_{n,i}\right)\hat{X}_{n,k}\,Y_n'(0) \tag{52}$$

and

$$SDR_2(\bar{t}) = \frac{2}{\sum_{k=1}^{N}\bar{L}_k}\sum_{k=1}^{N}\sum_{n=1}^{\infty}\left(\hat{\psi}_n + \hat{\psi}_{n,0} + \sum_{i=1}^{\infty}\hat{\psi}_{n,i}\right)\hat{X}_{n,k}\,Y_n'(\bar{w}_y) \tag{53}$$

HESSD
12, 7503–7540, 2015

with

$$Y_n'(\bar{y}) = \frac{\kappa_1 \beta_n \cos(\beta_n \bar{y}) - \beta_n^2 \sin(\beta_n \bar{y})}{(\beta_n^2 + \kappa_1^2)[\bar{w}_y + \kappa_2/(\beta_n^2 + \kappa_2^2)] + \kappa_1} \quad (54)$$

$$\hat{\psi}_n = -\{\sinh(\bar{z}_0 \lambda_n) \cosh[(1-\bar{z}_0)\lambda_n] + \sinh[(1-\bar{z}_0)\lambda_n] \cosh(\bar{z}_0 \lambda_n)\}/(\kappa_z \lambda_n^2 \sinh \lambda_n) \quad (55)$$

$$\hat{\psi}_{n,0} = -\mu_{n,0}(\theta_{n,0} + \vartheta_{n,0}) \,/\, \lambda_0 \quad (56)$$

$$\theta_{n,0} = \cosh\left[(1-\bar{z}_0)\lambda_0\right] \{p_0 \gamma[-1 + \cosh(\bar{z}_0 \lambda_0) + \kappa_z \lambda_0 \sinh(\bar{z}_0 \lambda_0)]\} \quad (57)$$

$$\vartheta_{n,0} = \sinh\left[(1-\bar{z}_0)\lambda_0\right] [\kappa_z \lambda_0 \cosh(\bar{z}_0 \lambda_0) + p_0 \gamma \sinh(\bar{z}_0 \lambda_0)] \quad (58)$$

$$\hat{\psi}_{n,i} = \nu_{n,i}(\sigma_{n,i} - \eta_{n,i}) \,/\, \lambda_i \quad (59)$$

$$\sigma_{n,i} = \cos\left[(1-\bar{z}_0)\lambda_i\right] \{p_i \gamma \left[-1 + \cos(\bar{z}_0 \lambda_i)\right] - \kappa_z \lambda_i \sin(\bar{z}_0 \lambda_i)\} \quad (60)$$

$$\eta_{n,i} = \sin\left[(1-\bar{z}_0)\lambda_i\right] \left[\kappa_z \lambda_i \cos(\bar{z}_0 \lambda_i) + p_i \gamma \sin(\bar{z}_0 \lambda_i)\right] \quad (61)$$

where $\lambda_n = \beta_n / \sqrt{\kappa_z}$; $p_0 = \kappa_z \lambda_0^2 - \beta_n^2$; $p_i = -\kappa_z \lambda_i^2 - \beta_n^2$; $\mu_{n,0}$ equals $\mu_{m,n,0}$ in Eq. (36) with $\alpha_m = 0$; $\nu_{n,i}$ equals $\nu_{m,n,i}$ in Eq. (37) with $\alpha_m = 0$; $\hat{X}_{n,k}$ is defined in Eq. (45) for $\theta_k \neq 0$ or π and Eq. (49) for $\theta_k = 0$ or π; and λ_0 and λ_i are the roots of Eqs. (40) and (41) with $\alpha_m = 0$, respectively.

2.6 Special cases of the present solution

2.6.1 Confined aquifer of finite extent

If $\gamma = 0$ (i.e.,$S_y = 0$ in Eq. 8), the top boundary is regarded as an impermeable stratum. The aquifer system is then under the confined condition. Under this circumstance, Eq. (40) reduces to $e^{2\lambda_0} = 1$ having the root of $\lambda_0 = 0$, and Eq. (41) yields $\tan \lambda_i = 0$ having the roots of $\lambda_i = i\pi$ where $i \in 1, 2, 3, \ldots \infty$. With $\gamma = 0$, $\lambda_0 = 0$ and $\lambda_i = i\pi$, the head solution for a confined aquifer can be expressed as Eq. (44) with Eqs. (31)–(38) and (45)–(49) where $\psi_{m,n,0}$ in Eq. (32) is replaced by

$$\psi_{m,n,0} = -\exp\left(p_0 \bar{t}\right) / p_0 \quad (62)$$

HESSD
12, 7503–7540, 2015

Similarly, the SDR solution for a confined aquifer can be written as Eqs. (52) and (53) where $\hat{\psi}_{n,0}$ is replaced by Eq. (62).

2.6.2 Confined aquifer of infinite extent

The head solution introduced in Sect. 2.6.1 is applicable to spatiotemporal head distributions in confined aquifers of infinite extent before the lateral boundary effect comes. Wang and Yeh (2008) indicated that the time can be quantified, in our notation, as $t = R^2 S_s/(16K_y)$ (i.e., $\bar{t} = R^2/(16y_0^2)$ for dimensionless time) where R is the shortest distance between a RCW and aquifer lateral boundary. Prior to the time, the present head solution with $N = 1$ for a horizontal well in a confined aquifer gives very close results given in Zhan et al. (2001).

2.6.3 Unconfined aquifer of infinite extent

Prior to the beginning time mentioned in Sect. 2.6.2, the absolute value calculated by the present head solution, Eqs. (44) with $N = 1$, represents drawdown induced by a horizontal well in unconfined aquifers of infinite extent. The calculated drawdown should be close to that from Zhan and Zlotnik (2002) solution for the case of the instantaneous drainage from water table decline.

2.6.4 Unconfined aquifer of semi-infinite extent

When $\kappa_1 \to \infty$ (i.e., $b_1 = 0$), Eq. (14) reduces to the Dirichlet condition of $\bar{h} = 0$ for stream 1 in the absence from a low-permeability streambed, and Eq. (19) becomes ${}_{\kappa}\tan\left(\beta_n \bar{w}_y\right) = -\beta_n/_2$. In addition, the boundary effect occurring at the other three sides of the aquifer can be neglected prior to the beginning time. Moreover, when $N = 1$ and $\theta_1 = 0$, a RCW can be regarded as a horizontal well parallel to stream 1. Under these three conditions, the present head and SDR predictions are close to those in Huang et al. (2011), the head solution of which agrees well with measured data from a field experiment executed by Mohamed and Rushton (2006). On the other hand, before the

HESSD
12, 7503–7540, 2015

time when the boundary effect occurs at $\bar{x} = 0$, $\bar{x} = \bar{w}_x$ and $\bar{y} = \bar{w}_y$, the present head and SDR solutions for a RCW give close predictions to those in Huang et al. (2012), the head and SDR solutions of which agree well with observation data taken from two field experiments carried out by Schafer (2006) and Jasperse (2009), respectively.

2.7 Sensitivity analysis

The hydraulic parameters determined from field observed data are inevitably subject to measurement errors. Consequently, head predictions from the analytical model have uncertainty due to the propagation of measurement errors. Sensitivity analysis can be considered as a tool of exploring the response of the head to the change in a specific parameter (Zheng and Bennett, 2002). One may define the normalized sensitivity coefficient as

$$S_{i,t} = \frac{P_i}{H}\frac{\partial h}{\partial P_i} \tag{63}$$

where $S_{i,t}$ is the normalized sensitivity coefficient for the ith parameter at time t, and P_i represents the magnitude of the ith parameter. Eq. (63) can be approximated as

$$S_{i,t} = \frac{h(P_i + \Delta P_i) - h(P_i)}{\Delta P_i} \times \frac{P_i}{H} \tag{64}$$

where ΔP_i is an increment chosen as $10^{-3}P_i$ (Yeh et al., 2008).

3 Results and discussion

This section demonstrates head and SDR predictions and explores some physical insights regarding flow behavior. In Sect. 3.1, groundwater flow and equipotential lines induced by pumping are discussed. In Sect. 3.2, the influence of anisotropy on spatial

HESSD
12, 7503–7540, 2015

head and temporal SDR distributions is studied. In Sect. 3.3, the sensitivity analysis is performed to investigate the response of the head to the change in each hydraulic parameter. In Sect. 3.4, the effects of the vertical flow and well depth on temporal SDR distributions for confined and unconfined aquifers are investigated. In these sections, the default values for the parameters and variables are $b_1 = b_2 = 1\,\mathrm{m}$, $H = 20\,\mathrm{m}$, $Q = 100\,\mathrm{m^3\,day^{-1}}$, $S_s = 10^{-5}\,\mathrm{m^{-1}}$, $S_y = 0.2$, $K_1 = K_2 = 0.1\ \mathrm{m\,day^{-1}}$, $K_x = K_y = 1\,\mathrm{m\,day^{-1}}$, $K_z = 0.1\,\mathrm{m\,day^{-1}}$, $w_x = w_y = 800\,\mathrm{m}$, $x_0 = y_0 = 400\,\mathrm{m}$, and $z_0 = 10\,\mathrm{m}$. For conciseness, we consider a RCW with two laterals with $N = 2$, $L_1 = L_2 = 200\,\mathrm{m}$, $\theta_1 = 0$ and $\theta_2 = \pi$. The well can be viewed as a horizontal well having 400 m length and parallel to streams 1 and 2. The corresponding dimensionless parameters are $\bar{L}_1 = \bar{L}_2 = 0.5$, $\bar{w}_x = \bar{w}_y = 2$, $\gamma = 100$, $\bar{x}_0 = 1$, $\bar{z}_0 = 0.5$, $\kappa_x = \kappa_z = 1$, and $\kappa_1 = \kappa_2 = 20$.

3.1 Groundwater flow and hydraulic head

Most existing models assume 2-D flow with neglecting the vertical flow component for pumping at a horizontal well (e.g., Mohamed and Rushton, 2006; Haitjema et al., 2010). The head distributions predicted by those models are inaccurate if the observation well is close to the region where the vertical flow prevails. Figure 2 demonstrates the streamlines and equipotential lines predicted by the present solution for a horizontal well in an unconfined aquifer for $\bar{y} = 1$, $\bar{t} = 10^7$, $\kappa_x = 1$ and $\kappa_z = 0.1$, 1, and 10. The well is located at $9.5 \le \bar{x} \le 10.5$, $\bar{y}_0 = 1$ and $\bar{z}_0 = 0.5$ as illustrated in the figure. The stream function ψ can be derived via the Cauchy-Riemann equation, in our notation, as

$$\frac{\partial \bar{\psi}}{\partial \bar{x}} = -\sqrt{\kappa_z}\frac{\partial \bar{h}}{\partial \bar{z}} \tag{65}$$

where $\bar{\psi} = K_y H/Q$ is the dimensionless stream function. The function $\bar{\psi}$ is obtained firstly by substituting the present solution into Eq. (65), then by differentiating the result with respect to $\bar{z}$, and eventually by integrating the differentiation result to $\bar{x}$. The coefficient arising from the integration is determined by the condition of $\bar{\psi} = 0$ at $\bar{x} = \bar{x}_0$.

HESSD
12, 7503–7540, 2015

When $\kappa_z = 0.1$, in the range of $10 \le \bar{x} \le 13.66$, the contours of the hydraulic head are in a curved path, and the flow toward the well is slanted. Moreover, the range decreases to $10 \le \bar{x} \le 11.5$ when $\kappa_z = 1$ and to $10 \le \bar{x} \le 10.82$ when $\kappa_z = 10$. Beyond these ranges, the head contours are nearly vertical, and the flow is essentially horizontal. Define $\bar{d} = d/y_0$ as a shortest dimensionless horizontal distance between the well and a nearest location of only horizontal flow. The $\bar{d}$ is therefore chosen as 3.16, 1 and 0.32 for the cases of $\kappa_z = 0.1$, 1 and 10, respectively. Substituting $(\kappa_z, \bar{d}) = (0.1, 3.16)$, (1, 1) and (10, 0.32) into $\kappa_z \bar{d}^2$ leads to about unity. We may therefore conclude that the vertical flow component is negligible if $\kappa_z \bar{d}^2 \ge 1$ (i.e., $\ge K_z d^2/(K_y H^2)$ 1) for thin aquifers, observation locations far from the well, and/or a large ratio of K_z/K_y.

3.2 Anisotropy analysis of hydraulic head and stream depletion rate

Previous articles have seldom analyzed flow behavior for anisotropic aquifers, i.e., κ_x $(K_x/K_y) \ne 1$. Head predictions based on the models, developed for isotropic aquifers, will be inaccurate if $\kappa_x \ne 1$. Consider $\bar{w}_x = \bar{w}_y = 2$, $\bar{t} = 10^7$ for steady-state head distributions, and a RCW with $\bar{L}_1 = \bar{L}_2 = 0.25$, $\theta_1 = 0$, $\theta_2 = \pi$, and $(\bar{x}_0 \bar{y}_0 \bar{z}_0) = (1, 1, -0.5)$ for symmetry. The contours of the dimensionless head at $\bar{z} = -0.5$ are shown in Fig. 3a–d for $\kappa_x = 1$, 10 and 50, 10^{-3}, and 10^{-4}, respectively. The figure indicates that the anisotropy causes a significant effect on the head distributions in comparison with the case of $\kappa_x = 1$. In Fig. 3b, the contours exhibit smooth curves in the strap regions of $1 \le \bar{y} \le 1.45$ for the case of $\kappa_x = 10$ and $1 \le \bar{y} \le 1.2$ for the case of $\kappa_x = 50$. For the region of $\bar{y} \ge 1.45$, the predicted heads for both cases agree well, and all the contour lines are parallel, indicating that the flow is essentially unidirectional. Substituting $(\kappa_x, \bar{y}) = (10, 1.45)$ and (50, 1.2) into $\kappa_x (\bar{y} - 1)^2$ results in a value about 2. Accordingly, we may draw the conclusion that plots from the inequality of $\kappa_x (\bar{y} - 1)^2 \le 2$ indicate the strap region for κ_x being greater than 10. Some existing models assuming 2-D flow in a vertical plane with neglecting the flow component along a horizontal well give accurate head

HESSD
12, 7503–7540, 2015

predictions beyond the region (e.g., Anderson, 2000; Anderson, 2003; Kompani-Zare et al., 2005).

Aquifers with $K_y H \geq 10^3\ \mathrm{m^2\ day^{-1}}$ can efficiently produce plenty of water from a well. RCWs usually operate with $Q \leq 10^5\ \mathrm{m^3\ day^{-1}}$ for field experiments (e.g., Schafer, 2006; Jasperse, 2009). We therefore define significant dimensionless head drop as $|\bar{h}| > 10^{-5}$ (i.e., $|h| > 1$ mm). The anisotropy of $\kappa_x < 1$ produces the drop in the strap areas of $1 \leq \bar{x} \leq 1.48$ for the case of $\kappa_x = 10^{-3}$ in Fig. 3c and $1 \leq \bar{y} \leq 1.32$ for the case of $\kappa_x = 10^{-4}$ in Fig. 3d. Substituting $(\kappa_x, \bar{x}) = (10^{-3}, 1.48)$ and $(10^{-4}, 1.32)$ into $(\bar{x} - \bar{x}_0 - \bar{L}_1)^2/\kappa_x$ approximates 52.9. This result leads to the conclusion that the area can be determined by the inequalities of $(\bar{x} - \bar{x}_0 - \bar{L}_1)^2 \leq 52.9\kappa_x$ and $(\bar{x} - \bar{x}_0 + \bar{L}_2)^2 \leq 52.9\kappa_x$ for any value of κ_x in the range $\kappa_x < 1$. For a RCW with irregular lateral configurations, the inequalities become $(\bar{x} - \max\bar{x}_k)^2 \leq 52.9\kappa_x$ and $(\bar{x} - \min\bar{x}_k)^2 \leq 52.9\kappa_x$ where $\bar{x}_k$ is coordinate $\bar{x}$ of the far end of the k-th lateral. The conclusion applies in principle to reduction in grid points for numerical solutions based on finite difference methods or finite element methods. On the other hand, we have found that Eq. (52) or (53) with various κ_x predicts the same temporal SDR distribution (not shown), indicating that the SDR is independent of κ_x.

3.3 Sensitivity analysis of hydraulic head

Consider two piezometers at point A of (400, 340, −10 m) and point B of (400, 80, −10 m) as illustrated in Fig. 4. As discussed in Sect. 3.1, the temporal head distribution at point A exhibits the unconfined behavior in Fig. 4a because of $\kappa_z\, \bar{d}^2 < 1$ while at point B displays the confined one in Fig. 4b due to $\kappa_z \bar{d}^2 > 1$. The sensitivity analysis is conducted with the aid of Eq. (64) to observe head responses at these two piezometers to the change in each of K_x, K_y, K_z, S_s, S_y, K_1, L_1 and z_0. The temporal distribution curves of the normalized sensitivity coefficients for those eight parameters are shown in Fig. 4a for point A and 4b for point B. The figure demonstrates that the hydraulic heads at both piezometers are most sensitive to the change in K_y, second sensitive

HESSD
12, 7503–7540, 2015

to the change in K_x and thirdly sensitive to the change in S_y, indicating that K_y, K_x and S_y are the most crucial factors in designing a pumping system. This figure also shows that the heads at point A is sensitive to the change in S_s at the early period of 4×10^{-3} day $< t < 10^{-1}$ day but at point B is insensitive to the change over the entire period. In addition, the head at point A is sensitive to the changes in K_z and z_0 due to 3-D flow (i.e., $\kappa_z \bar{d}^2 < 1$) as discussed in Sect. 3.1. In contrast, the head at point B is insensitive to the changes in K_z and z_0 because the vertical flow diminishes (i.e., $\kappa_z \bar{d}^2 > 1$). Moreover, the head at point A is sensitive to the change in L_1 but the head at point B is not because its location is far away from the well. Furthermore, the normalized sensitivity coefficient of K_1 for point A away from stream 1 approaches zero but for point B in the vicinity of stream 1 increases with time and finally maintains a certain value at the steady state. Regarding the sensitivity analysis of SDR, Huang et al. (2014) has performed the sensitivity analysis of normalized coefficients of SDR_1 to the changes in K_y, K_1 and S_s for a confined aquifer and in K_y, K_z, K_1, S_s and S_y for an unconfined aquifer.

3.4 Effects of vertical flow and well depth on stream depletion rate

Huang et al. (2014) reveals that the effect of the vertical flow on SDR induced by a vertical well is dominated by the magnitude of the key factor κ_z (i.e., $K_z y_0^2/(K_y H^2)$) where y_0 herein is a distance between stream 1 and the vertical well. They concluded that the effect is negligible when $\kappa_z \geq 10$ for a leaky aquifer. The factor should be replaced by $\kappa_z \bar{a}^2$ (i.e., $K_z a^2/(K_y H^2)$) where a is a shortest distance measured from stream 1 to the end of a lateral of a RCW, and $\bar{a} = a/y_0 = 1$ in this study due to $N = 2$, $\theta_1 = 0$ and $\theta_2 = \pi$. We investigate SDR in response to various $\bar{z}_0$ and $\kappa_z \bar{a}$ for unconfined and confined aquifers. The temporal SDR_1 distributions predicted by Eq. (52) for stream 1 adjacent to an unconfined aquifer are shown in Fig. 5a for $\bar{z}_0 = 0.5$ and $\kappa_z \bar{a}^2 = 0.01$, 0.1, 1, 10, 20 and 30 and Fig. 5b for $\kappa_z \bar{a}^2 = 1$ and 30 when $\bar{z}_0 = 0.1$, 0.3, 0.5, 0.7 and 0.9. The curves of SDR_1 versus $\bar{t}$ is plotted in both panels by the present SDR solution for a

HESSD
12, 7503–7540, 2015

confined aquifer. In Fig. 5a, the present solution for an unconfined aquifer predicts a close SDR_1 to that for the confined aquifer when $\kappa_z\bar{a}^2 = 0.01$, indicating that the vertical flow in the unconfined aquifer is ignorable. The SDR_1 for the unconfined aquifer with $\kappa_z\bar{a}^2 = 30$ behaves like that for a confined one, indicating the vertical flow is also ignorable. The SDR_1 is therefore independent of well depths $\bar{z}_0$ when $\kappa_z\bar{a}^2 = 30$ as shown in Fig. 5b. We may therefore conclude that, under the condition of $\kappa_z\bar{a}^2 \leq 0.01$ or $\kappa_z\bar{a}^2 \geq 30$, a 2-D horizontal flow model can give good predictions in SDR_1 for unconfined aquifers. In contrast, SDR_1 increases with decreasing $\kappa_z\bar{a}^2$ when $0.01 < \kappa_z\bar{a}^2 < 30$ in Fig. 5a, indicating that the vertical flow component induced by pumping in unconfined aquifers significantly affects SDR_1. The effect of well depth $\bar{z}_0$ on SDR_1 is also significant as shown in Fig. 5b when $\kappa_z\bar{a}^2 = 1$. Obviously, the vertical flow effect should be considered in a model when $0.01 < \kappa_z\bar{a}^2 < 30$ for unconfined aquifers.

It is interesting to note that the SDR_1 or SDR_2 induced by two laterals (i.e., $\theta_1 = 0$ and $\theta_2 = \pi$) parallel to the streams adjacent to a confined aquifer is independent of $\kappa_z\bar{a}^2$ and $\bar{z}_0$ but depends on aquifer width of $\bar{w}_y$. The temporal SDR distribution curves based on Eqs. (52) and (53) with $\gamma = 0$ for a confined aquifer with $\bar{w}_y = 2$, 4, 6, 10 and 20 are plotted in Fig. 6. The dimensionless distance between the well and stream 1 is set to unity for each case. The SDR_1 predicted by Hunt (1999) solution based on a vertical well in a confined aquifer extending infinitely is considered. The present solution for each $\bar{w}_y$ gives the same SDR_1 as the Hunt solution before the time when stream 2 contributes filtration water to the aquifer and influences the supply of SDR_1. It is interesting to note that the sum of steady-state SDR_1 and SDR_2 is always unity for a fixed $\bar{w}_y$. The former and latter can be estimated by $(\bar{w}_y - 1)/\bar{w}_y$ and $1/\bar{w}_y$, respectively. Such a result corresponds with that in Sun and Zhan (2007) which investigates the distribution of steady-state SDR_1 and SDR_2 induced by a vertical well.

HESSD
12, 7503–7540, 2015

4 Concluding remarks

This study develops a new analytical model describing 3-D flow induced by a RCW in a rectangular confined or unconfined aquifer bounded by two parallel streams and no-flow stratums in the other two sides. The flow equation in terms of the hydraulic head with a point sink term is employed. Both streams fully penetrate the aquifer and are under the Robin condition in the presence of low-permeability streambeds. A first-order free surface equation is used to describe the water table decline. The head solution for the point sink is expressed in terms of a triple series derived by the methods of Laplace transform and double-integral transform. The head solution for a RCW is then obtained by integrating the point-sink solution along the laterals and dividing the integration result by the sum of lateral lengths. On the basis of Darcy's law and the head solution, the SDR solution for two streams can also be acquired. The sensitivity analysis is performed to explore the response of the head to the change in each of the hydraulic parameters and variables. New findings regarding the responses of flow and SDR to pumping at a RCW are summarized below:

1. In the region of $\bar{d} < \sqrt{1/\kappa_z}$ for unconfined aquifers, groundwater flow is 3-D, and temporal head distributions exhibit the unconfined behavior. A mathematical model should consider 3-D flow when predicting the hydraulic head in this region. Beyond this region, groundwater flow is horizontal, and temporal head distributions display the confined behavior. A 2-D flow model can predict accurate hydraulic head.

2. The aquifer anisotropy of $\kappa_x > 10$ causes unidirectional flow in the strap region determined based on $\kappa_x(\bar{y}-1)^2 > 2$ for a horizontal well. Existing models assuming 2-D flow in a vertical plane with neglecting the flow component along the well give accurate head predictions beyond the region.

HESSD
12, 7503–7540, 2015

3. The aquifer anisotropy of $\kappa_x < 1$ produces significant change in the head (i.e., $|\bar{h}| > 10^{-5}$ or $|h| > 1$ mm) in the strap area determined by $(\bar{x} - \max\bar{x}_k)^2 \le 52.9\kappa_x$ and $(\bar{x} - \min\bar{x}_k)^2 \le 52.9\kappa_x$ for a RCW with irregular lateral configurations.

4. The hydraulic head in the whole domain is most sensitive to the change in K_y, second sensitive to the change in K_x, and thirdly sensitive to the change in S_s. They are thus the most crucial factors in designing a pumping system.

5. The hydraulic head is sensitive to changes in K_z, S_s, z_0 and L_k in the region of $\bar{d} < \sqrt{1/\kappa_z}$ and is insensitive to the changes of them beyond the region.

6. The hydraulic head at observation locations near stream 1 is sensitive to the change in K_1 but away from the stream isn't.

7. The effect of the vertical flow on SDR can be ignored when $\kappa_z\bar{a}^2 \le 0.01$ or $\kappa_z\bar{a}^2 \ge 30$ for unconfined aquifers. In contrast, neglecting the effect will underestimate SDR when $0.01 < \kappa_z\bar{a}^2 < 30$.

8. For unconfined aquifers, SDR increases with dimensionless well depth $\bar{z}_0$ when $0.01 < \kappa_z < 30$ and is i ndependent of $\bar{z}_0$ when $\kappa_z \le 0.01$ or $\kappa_z \ge 30$. For confined aquifers, SDR is independent of $\bar{z}_0$ and κ_z. For both kinds of aquifers, the distribution curve of SDR versus $\bar{t}$ is independent of aquifer anisotropy κ_x.

Appendix A: Double-integral transform

Latinopoulos (1985) provided the double-integral transform for a rectangular aquifer domain where each side can be under either the Dirichlet, no-flow, or Robin condition.

HESSD
12, 7503–7540, 2015

The transform corresponding to the boundary conditions, Eqs. (12)–(15) is defined as

$$\widetilde{h}(\alpha_m,\beta_n)=\Im\left\{\bar{h}(\bar{x},\bar{y})\right\}=\int_0^{\bar{w}_x}\int_0^{\bar{w}_y}\bar{h}(\bar{x},\bar{y})\cos(\alpha_m\bar{x})K(\bar{y})\,d\bar{y}\,d\bar{x} \tag{A1}$$

with

$$K(\bar{y})=\sqrt{2}\frac{\beta_n\cos(\beta_n\bar{y})+\kappa_1\sin(\beta_n\bar{y})}{\sqrt{(\beta_n^2+\kappa_1^2)[\bar{w}_y+\kappa_2/(\beta_n^2+\kappa_2^2)]+\kappa_1}} \tag{A2}$$

where $\cos(\alpha_m\bar{x})K(\bar{y})$ is the kernel function. According to Latinopoulos (1985, Eq. 9), the transform has the property of

$$\Im\left\{\kappa_x\frac{\partial^2\bar{h}}{\partial\bar{x}^2}+\frac{\partial^2\bar{h}}{\partial\bar{y}^2}\right\}=-(\kappa_x\alpha_m^2+\beta_n^2)\widetilde{h}(\alpha_m,\beta_n) \tag{A3}$$

The formula for the inverse double-integral transform can be written as (Latinopoulos, 1985, Eq. 14)

$$\bar{h}(\bar{x},\bar{y})=\Im^{-1}\left\{\widetilde{h}(\alpha_m,\beta_n)\right\}=\frac{1}{\bar{w}_x}\left[\sum_{n=1}^{\infty}\widetilde{h}(0,\beta_n)K(\bar{y})+2\sum_{m=1}^{\infty}\sum_{n=1}^{\infty}\widetilde{h}(\alpha_m,\beta_n)\cos(\alpha_m\bar{x})K(\bar{y})\right] \tag{A4}$$

Appendix B: Derivation of Eq. (31)

The RHS term of Eq. (28) is a single-value function with respect to p. On the basis of the residue theorem, the inverse Laplace transform for Eq. (28) equals the summation of residues of poles in the complex plane. The residue of a simple pole can be derived according to the formula below:

$$\mathrm{Res}|_{p=p_i}=\lim_{p\to p_i}\Omega(a,b,c)(p-p_i) \tag{B1}$$

HESSD
12, 7503–7540, 2015

where p_i is the location of the pole in the complex plane.

The locations of poles are the roots of the equation obtained by letting the denominator of Eq. (28) to be zero, denoted as

$$p\,\kappa_z\,\lambda\,(p\,\gamma\cosh\lambda + \kappa_z\,\lambda\sinh\lambda) = 0 \tag{B2}$$

where λ is defined in Eq. (29). Notice that $p = -\kappa_x\alpha_m^2 - \beta_n^2$ obtained by $\lambda = 0$ is not a pole in spite of being a root.

Apparently, one pole is at $p = 0$, and the residue based on Eq. (B1) equals the RHS function in Eq. (33). Other poles are determined by the equation of

$$p\,\gamma\cosh\lambda + \kappa_z\,\lambda\sinh\lambda = 0 \tag{B3}$$

which comes from Eq. (B2). One pole is at $p = p_0$ between $p = 0$ and $p = -\kappa_x\,\alpha_m^2 - \beta_n^2$ in the negative part of the real axis. According to Eq. (29), we let $\lambda = \lambda_0$ and then have $p = \kappa_z\,\lambda_0^2 - \kappa_x\,\alpha_m^2 - \beta_n^2$. Substituting $\lambda = \lambda_0$ and $p = \kappa_z\,\lambda_0^2 - \kappa_x\,\alpha_m^2 - \beta_n^2$ into Eq. (B3) leads to Eq. (40). The location $p = p_0$ of the simple pole can be acquired by substituting the root of Eq. (40) into $p_0 = \kappa_z\,\lambda_0^2 - \kappa_x\,\alpha_m^2 - \beta_n^2$. The residue of the simple pole at $p = p_0$ equals the RHS function in Eq. (34). On the other hand, infinite poles are at $p = p_i$ behind $p = -\kappa_x\,\alpha_m^2 - \beta_n^2$. In light of Eq. (29), we let $\lambda = \sqrt{-1}\lambda_i$ and then have $p = -\kappa_z\,\lambda_i^2 - \kappa_x\,\alpha_m^2 - \beta_n^2$ for the absence of the imaginary unit. Substituting $\lambda = \sqrt{-1}\lambda_i$ and $p = -\kappa_z\,\lambda_i^2 - \kappa_x\,\alpha_m^2 - \beta_n^2$ into Eq. (B3) results in Eq. (41). The locations $p = p_i$ of those simple poles are obtained via the roots of Eq. (41) and $p_i = -\kappa_z\,\lambda_i^2 - \kappa_x\,\alpha_m^2 - \beta_n^2$. The residues of those simple poles at $p = p_i$ equal the RHS function in Eq. (35). Eventually, applying the formula for the inverse double-integral transform, Eq. (A4), to the sum of those residues in Eq. (32) yields Eq. (31).

Acknowledgements. Research leading to this paper has been partially supported by the grants from the Taiwan Ministry of Science and Technology under the contract NSC 102 – 2221 – E – 009 – 072 – MY2, MOST 103 – 2221 – E – 009 – 156, and MOST 104 – 2221 – E – 009 – 148 – MY2.

HESSD
12, 7503–7540, 2015

References

Anderson, E. I.: The method of images for leaky boundaries, Adv. Water Resour., 23, 461–474, doi:10.1016/S0309-1708(99)00044-5, 2000.

Anderson, E. I.: An analytical solution representing groundwater-surface water interaction, Water Resour. Res., 39, 1071, doi:10.1029/2002WR001536, 2003.

Anderson, E. I.: Stable pumping rates for horizontal wells in bank filtration systems, Adv. Water Resour., 54, 57–66, doi:10.1016/j.advwatres.2012.12.012, 2013.

Chen, C. X., Wan, J. W., and Zhan, H. B.: Theoretical and experimental studies of coupled seepage-pipe flow to a horizontal well, J. Hydrol., 281, 159–171, doi:10.1016/S0022-1694(03)00207-5, 2003.

Chen, X., Dong, W., Ou, G., Wang, Z., and Liu, C.: Gaining and losing stream reaches have opposite hydraulic conductivity distribution patterns, Hydrol. Earth Syst. Sci., 17, 2569–2579, doi:10.5194/hess-17-2569-2013, 2013.

Exner-Kittridge, M., Salinas, J. L., and Zessner, M.: An evaluation of analytical stream to groundwater exchange models: a comparison of gross exchanges based on different spatial flow distribution assumptions, Hydrol. Earth Syst. Sci., 18, 2715–2734, doi:10.5194/hess-18-2715-2014, 2014.

Flipo, N., Mouhri, A., Labarthe, B., Biancamaria, S., Rivière, A., and Weill, P.: Continental hydrosystem modelling: the concept of nested stream–aquifer interfaces, Hydrol. Earth Syst. Sci., 18, 3121–3149, doi:10.5194/hess-18-3121-2014, 2014.

Haitjema, H., Kuzin, S., Kelson, V., and Abrams, D.: Modeling flow into horizontal wells in a Dupuit-Forchheimer model, Ground Water, 48, 878–883, doi:10.1111/j.1745-6584.2010.00694.x, 2010.

Hantush, M. S. and Papadopoulos, I. S.: Flow of groundwater to collector wells, J. Hydr. Eng. Div., 88, 221–244, 1962.

Huang, C. S., Chen, Y. L., and Yeh, H. D.: A general analytical solution for flow to a single horizontal well by Fourier and Laplace transforms, Adv. Water Resour., 34, 640–648, doi:10.1016/j.advwatres.2011.02.015, 2011.

Huang, C. S., Tsou, P. R., and Yeh, H. D.: An analytical solution for a radial collector well near a stream with a low-permeability streambed, J. Hydrol., 446, 48–58, doi:10.1016/j.jhydrol.2012.04.028, 2012.

HESSD
12, 7503–7540, 2015

Huang, C. S., Lin, W. S., and Yeh, H. D.: Stream filtration induced by pumping in a confined, unconfined or leaky aquifer bounded by two parallel streams or by a stream and an impervious stratum, J. Hydrol., 513, 28–44, doi:10.1016/j.jhydrol.2014.03.039, 2014.
Hunt, B.: Unsteady stream depletion from ground water pumping, Ground Water, 37, 98–102, doi:10.1111/j.1745-6584.1999.tb00962.x, 1999.
Hunt, B.: Flow to vertical and nonvertical wells in leaky aquifers, J. Hydrol. Eng., 10, 477–484, doi:10.1061/(ASCE)1084-0699(2005)10:6(477), 2005.
Jasperse, J.: Planning, design and operations of collector 6, Sonoma County Water Agency, NATO Sci. Peace Secur., 169–202, doi:10.1007/978-94-007-0026-0_ 11, 2009.
Kawecki, M. W.: Transient flow to a horizontal water well, Ground Water, 38, 842–850, doi:10.1111/j.1745-6584.2000.tb00682.x, 2000.
Kawecki, M. W. and Al-Subaikhy, H. N.: Unconfined linear flow to a horizontal well, Ground Water, 43, 606–610, doi:10.1111/j.1745-6584.2005.0059.x, 2005.
Kompani-Zare, M., Zhan, H., and Samani, N.: Analytical study of capture zone of a horizontal well in a confined aquifer, J. Hydrol., 307, 48–59, doi:10.1016/j.jhydrol.2004.09.021, 2005.
Latinopoulos, P.: Analytical solutions for periodic well recharge in rectangular aquifers with third-kind boundary conditions, J. Hydrol., 77, 293–306, 1985.
Lee, E., Hyun, Y., Lee, K. K., and Shin, J.: Hydraulic analysis of a radial collector well for riverbank filtration near Nakdong River, South Korea, Hydrogeol. J., 20, 575–589, doi:10.1007/s10040-011-082-3, 2012.
Mohamed, A. and Rushton, K.: Horizontal wells in shallow aquifers: Field experiment and numerical model, J. Hydrol., 329, 98–109, doi:10.1016/j.jhydrol.2006.02.006, 2006.
Nyholm, T., Christensen, S., and Rasmussen, K. R.: Flow depletion in a small stream caused by ground water abstraction from wells, Ground Water, 40, 425–437, 2002.
Park, E. and Zhan, H. B.: Hydraulics of a finite-diameter horizontal well with wellbore storage and skin effect, Adv. Water Resour., 25, 389–400, doi:10.1016/S0309-1708(02)00011-8, 2002.
Park, E. and Zhan, H. B.: Hydraulics of horizontal wells in fractured shallow aquifer systems, J. Hydrol., 281, 147–158, doi:10.1016/S0022-1694(03)00206-3, 2003.
Rodríguez, L., Vives, L., and Gomez, A.: Conceptual and numerical modeling approach of the Guarani Aquifer System, Hydrol. Earth Syst. Sci., 17, 295–314, doi:10.5194/hess-17-295-2013, 2013.

HESSD
12, 7503–7540, 2015

Rushton, K. R. and Brassington, F. C.: Significance of hydraulic head gradients within horizontal wells in unconfined aquifers of limited saturated thickness, J. Hydrol., 492, 281–289, doi:10.1016/j.jhydrol.2013.04.006, 2013a.

Rushton, K. R. and Brassington, F. C.: Hydraulic behavior and regional impact of a horizontal well in a shallow aquifer: example from the Sefton Coast, northwest England (UK), Hydrogeol. J., 21, 1117–1128, doi:10.1007/s10040-013-0985-0, 2013b.

Schafer, D. C.: Use of aquifer testing and groundwater modeling to evaluate aquifer/river hydraulics at Louisville Water Company, Louisville, Kentucky, USA, NATO Sci. Ser. IV Earth Enviro. Sci., 60, 179–198, doi:10.1007/978-1-4020-3938-6_ 8, 2006.

Steward, D. R.: Threedimensional analysis of the capture of contaminated leachate by fully penetrating, partially penetrating, and horizontal wells, Water Resour. Res., 35, 461–468, doi:10.1029/1998WR900022, 1999.

Su, G. W., Jasperse, J., Seymour, D., Constantz, J., and Zhou, Q.: Analysis of pumping-induced unsaturated regions beneath a perennial river, Water Resour. Res., 43, W08421, doi:10.1029/2006WR005389, 2007.

Sun, D. M. and Zhan, H. B.: Flow to a horizontal well in an aquitard-aquifer system, J. Hydrol., 321, 364–376, doi:10.1016/j.jhydrol.2005.08.008, 2006.

Sun, D. M. and Zhan, H. B.: Pumping induced depletion from two streams, Adv. Water Resour., 30, 1016–1026, doi:10.1016/j.advwatres.2006.09.001, 2007.

Todd, D. K. and Mays, L. W.: Groundwater hydrology, John Wiley & Sons, Inc., New Jersey, USA, 240, 2005.

Tsou, P.-R., Feng, Z.-Y., Yeh, H.-D., and Huang, C.-S.: Stream depletion rate with horizontal or slanted wells in confined aquifers near a stream, Hydrol. Earth Syst. Sci., 14, 1477–1485, doi:10.5194/hess-14-1477-2010, 2010.

Unland, N. P., Cartwright, I., Cendón, D. I., and Chisari, R.: Residence times and mixing of water in river banks: implications for recharge and groundwater-surface water exchange, Hydrol. Earth Syst. Sci., 18, 5109–5124, doi:10.5194/hess-18-5109-2014, 2014.

Wang, C. T. and Yeh, H. D.: Obtaining the steady-state drawdown solutions of constant-head and constant-flux tests, Hydrol. Process., 22, 3456–3461, doi:10.1002/hyp.6950, 2008.

Yeh, H. D. and Chang, Y. C.: Recent advances in modeling of well hydraulics, Adv. Water Resour., 51, 27–51, doi:10.1016/j.advwatres.2012.03.006, 2013.

HESSD
12, 7503–7540, 2015

Yeh, H. D., Chang, Y. C., and Zlotnik, V. A.: Stream depletion rate and volume from groundwater pumping in wedge-shaped aquifers, J. Hydrol., 349, 501–511, doi:10.1016/j.jhydrol.2007.11.025, 2008.
Yeh, H. D., Huang, C. S., Chang, Y. C., and Jeng, D. S.: An analytical solution for tidal fluctuations in unconfined aquifers with a vertical beach, Water Resour. Res., 46, W10535, doi:10.1029/2009WR008746, 2010.
Zhan, H. B. and Zlotnik, V. A.: Groundwater flow to a horizontal or slanted well in an unconfined aquifer, Water Resour. Res., 38, doi:10.1029/2001WR000401, 2002.
Zhan, H. B. and Park, E.: Horizontal well hydraulics in leaky aquifers, J. Hydrol., 281, 129–146, doi::10.1016/S0022-1694(03)00205-1, 2003.
Zhan, H. B., Wang, L. V., and Park, E.: On the horizontal-well pumping tests in anisotropic confined aquifers, J. Hydrol., 252, 37–50, doi:10.1016/S0022-1694(01)00453-X, 2001.
Zheng, C. and Bennett, G. D.: Applied contaminant transport modeling, 2nd ed., Wiley-Interscience, N.Y., 287, 2002.
Zhou, Y., Wenninger, J., Yang, Z., Yin, L., Huang, J., Hou, L., Wang, X., Zhang, D., and Uhlenbrook, S.: Groundwater-surface water interactions, vegetation dependencies and implications for water resources management in the semi-arid Hailiutu River catchment, China – a synthesis, Hydrol. Earth Syst. Sci., 17, 2435–2447, doi:10.5194/hess-17-2435-2013, 2013.
Zlotnik, V. A.: A concept of maximum stream depletion rate for leaky aquifers in alluvial valleys, Water Resour. Res., 40, W06507, doi:10.1029/2003WR002932, 2004.

HESSD
12, 7503–7540, 2015

Table 1. Symbols used in the text and their definitions.

Symbol	Definition
h	Hydraulic head
H	Aquifer thickness
Q	Pumping rate of point sink or RCW
t	Time since pumping
R	Shortest horizontal distance between the far end of lateral and aquifer lateral boundary
a	Shortest horizontal distance between stream 1 and the far end of lateral
d	Shortest horizontal distance between the far end of lateral and location of having only horizontal flow
N	The number of laterals
(x, y, z)	Cartesian coordinate system
(x_0', y_0', z_0')	Location of point sink
(x_0, y_0, z_0)	Location of center of RCW
(L_k, θ_k)	Length and counterclockwise angle from x axis to k-th lateral, respectively, where ($k \in 1, 2, \ldots N$)
(K_x, K_y, K_z)	Aquifer hydraulic conductivities in x, y and z directions, respectively
(S_s, S_y)	Specific storage and specific yield, respectively
(K_1, K_2)	Hydraulic conductivities of streambeds 1 and 2, respectively
(b_1, b_2)	Thicknesses of streambeds 1 and 2, respectively
(w_x, w_y)	Aquifer widths in x and y directions, respectively
$\bar{h}$	$(K_y H h)/Q$
$\bar{t}$	$(K_y t)/\left(S_s y_0^2\right)$
γ	$S_y/(S_s H)$
$\bar{L}_k$	L_k/y_0
$(\bar{x}, \bar{y}, \bar{z})$	$(x/y_0, y/y_0, z/H)$
$(\bar{x}_0', \bar{y}_0', \bar{z}_0')$	$(x_0'/y_0, y_0'/y_0, z_0'/H)$
$(\bar{x}_0, \bar{y}_0, \bar{z}_0)$	$(x_0/y_0, 1, z_0/H)$
$(\bar{d}, \bar{a})$	$(d/y_0, a/y_0)$
(κ_x, κ_z)	$(K_x/K_y, \left(K_z y_0^2\right)/\left(K_y H^2\right))$
(κ_1, κ_2)	$((K_1 y_0)/(K_y b_1), (K_2 y_0)/(K_y b_2))$
$(\bar{w}_x, \bar{w}_y)$	$(w_x/y_0, w_y/y_0)$
$\bar{x}_k$	Coordinate $\bar{x}$ of the far end of the k-th lateral
$(\max\bar{x}_k, \min\bar{x}_k)$	Maximum and minimum of $\bar{x}_k$, respectively, where $k \in 1, 2, \ldots N$

HESSD
12, 7503–7540, 2015

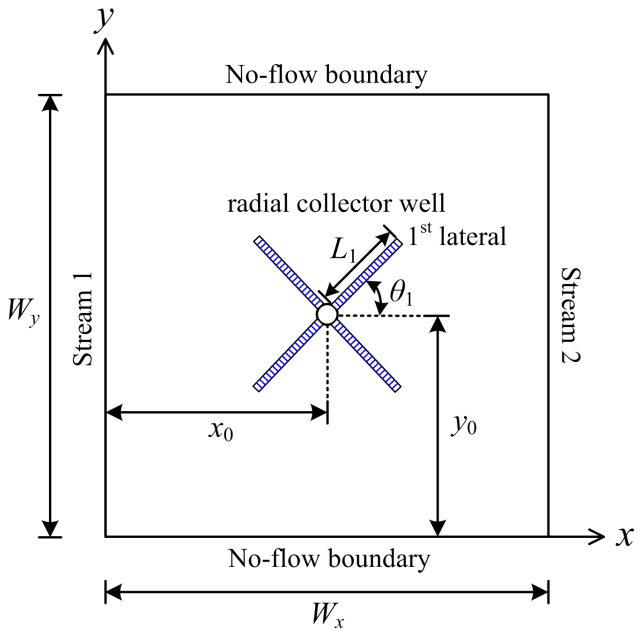

Figure 1. Schematic diagram of a radial collector well in a rectangular unconfined aquifer.

HESSD
12, 7503–7540, 2015

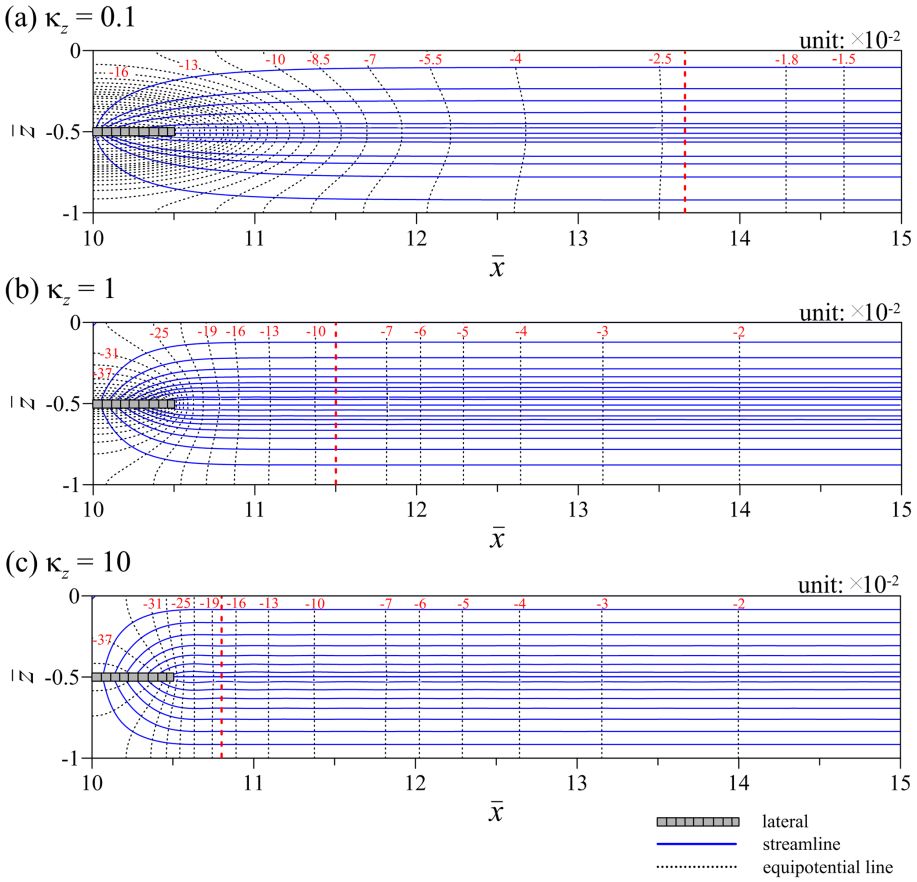

Figure 2. Streamlines and equipotential lines predicted by the present solution for κ_z = **(a)** 0.1, **(b)** 1 and **(c)** 10.

HESSD
12, 7503–7540, 2015

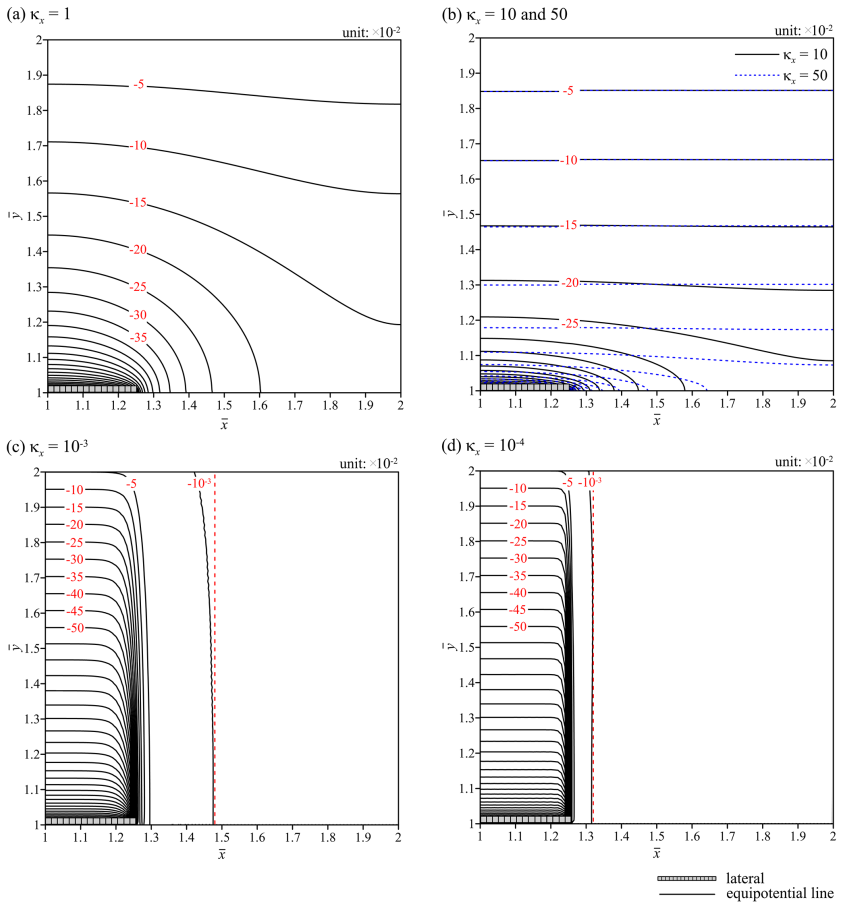

Figure 3. Spatial distributions of the dimensionless head predicted by the present head solution for κ_x = **(a)** 1, **(b)** 10 and 50, **(c)** 10^{-3} and **(d)** 10^{-4}.

HESSD
12, 7503–7540, 2015

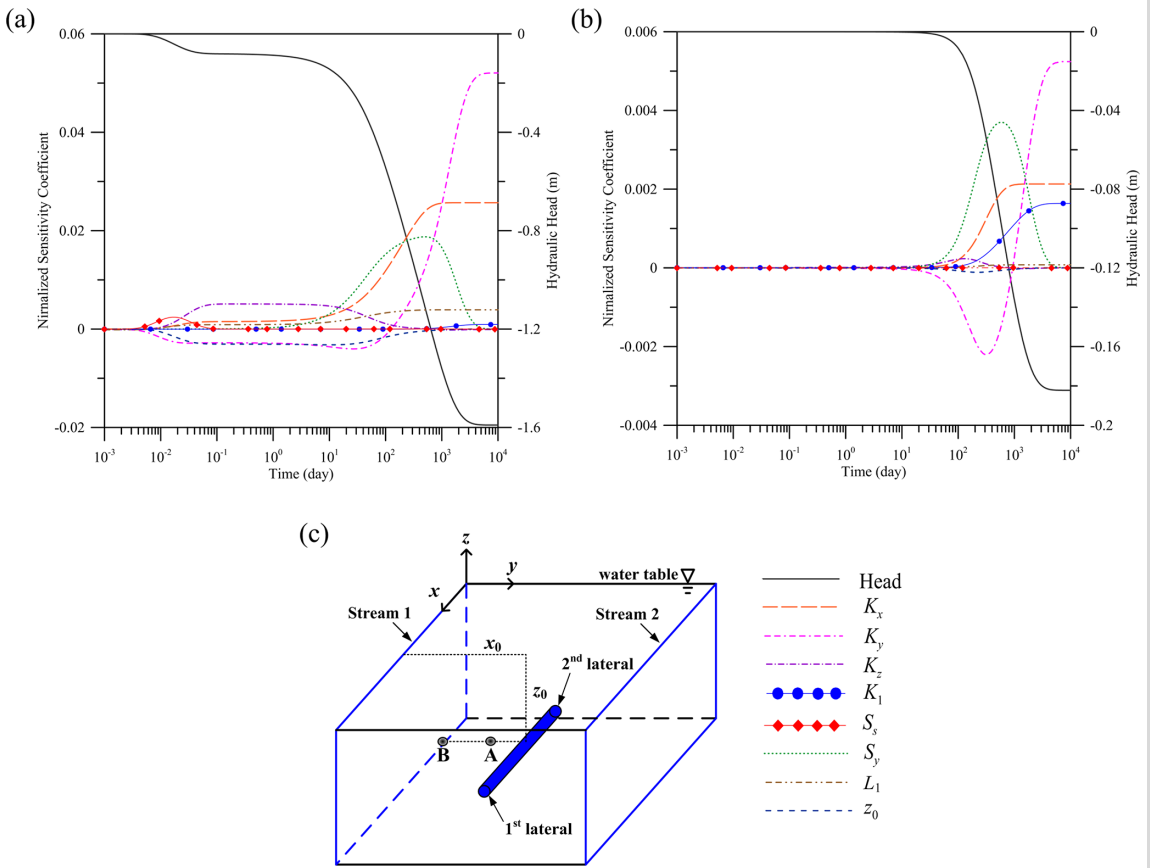

Figure 4. Temporal distribution curves of the normalized sensitivity coefficients for parameters K_x, K_y, K_z, S_s, S_y, K_1, L_1 and z_0 observed at piezometers **(a)** A of (400, 340, −10 m) and **(b)** B of (400, 80, −10 m).

HESSD
12, 7503–7540, 2015

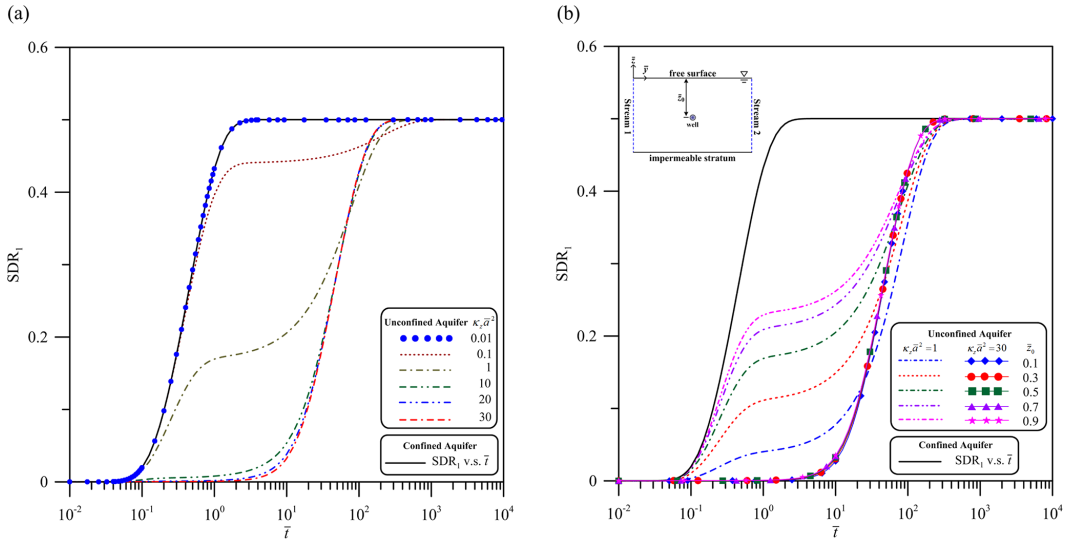

Figure 5. Temporal SDR_1 distributions predicted by Eq. (52) for stream 1 with various values of **(a)** $\kappa_z \bar{a}^2$ and **(b)** $\bar{z}_0$.

HESSD
12, 7503–7540, 2015

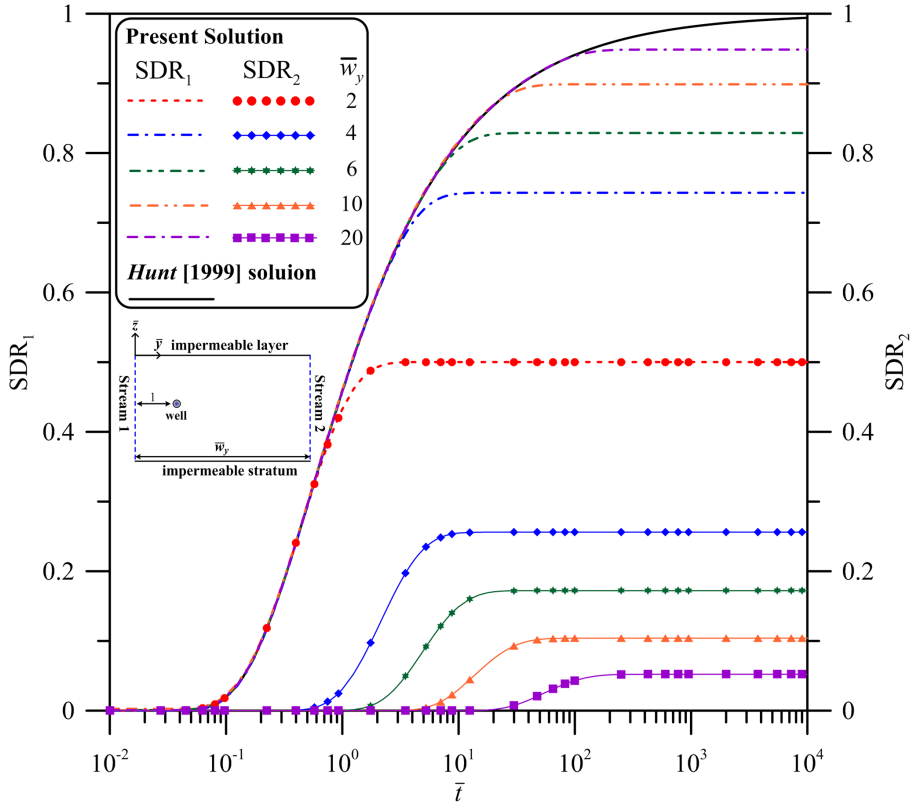

Figure 6. Temporal SDR distribution curves predicted by Eqs. (52) and (53) with $\gamma = 0$ for confined aquifers when $\bar{w}_y = 2$, 4, 6, 10 and 20.

HESSD
12, 7503–7540, 2015